Thickness and strain dependence of piezoelectric coefficient in $BaTiO_3$ thin films

K. P. Kelley,[1,*] D. E. Yilmaz,[3,*] L. Collins,[1] Y. Sharma,[2] H. N. Lee,[2] D. Akbarian,[3] A. C. T. van Duin,[3] P. Ganesh,[3,†] and R. K. Vasudevan[1]

[1]*The Center for Nanophase Materials Sciences, Oak Ridge National Laboratory, Oak Ridge, Tennessee 37831, USA*
[2]*Materials Science and Technology Division, Oak Ridge National Laboratory, Oak Ridge, Tennessee 37831, USA*
[3]*Deparment of Mechanical Engineering, The Pennsylvania State University, University Park, Pennsylvania 16802, USA*

(Received 24 September 2019; revised manuscript received 3 January 2020; accepted 9 January 2020; published 12 February 2020)

We explore the thickness dependence of the converse piezoelectric coefficient (d_{33}) in epitaxial thin films of $BaTiO_3$ (BTO) grown on (001) $SrTiO_3$ substrates. Piezoresponse force microscope was performed using an atomic force microscope equipped with an interferometric displacement sensor allowing direct quantification of electromechanical coupling coefficients in BTO free from unwanted background contributions. We find that 80-nm-thick films exhibit a d_{33} of ~ 20.5 pm/V, but as the thickness is reduced, the d_{33} reduces to less than 2 pm/V for a 10 nm film. To explain the atomistic origin of the effect, we performed molecular dynamics simulations with a recently developed *ab initio*-derived reactive force field, constructed using the ReaxFF framework. Simulations predict that under applied electric fields thin films of $BaTiO_3$ show an increasing thickness, with compressive strain, of the region screening the depolarization-field. This study confirms quantitatively the drop in piezoelectric performance in BTO ultrathin films and again highlights the importance of the screening mechanisms when films approach the ultrathin limits in dictating the functional behaviors.

DOI: 10.1103/PhysRevMaterials.4.024407

I. INTRODUCTION

The properties of ferroelectric films as they are scaled to the ultrathin limit has been a topic of considerable attention for decades, due to the novel physics that can arise [1,2]. Recently, it has been theoretically predicted, for example, that $BaTiO_3$ (BTO) thin films (below $\sim$30 nm) can exhibit highly peculiar phase diagrams when the electrochemical boundary conditions are properly considered, given that the surface electrochemical processes associated with screening can, at this thickness, have energies comparable with that from the bulk free energy arising from the polarization of the lattice [3,4]. Other work has shown, for example, experimentally that ultrathin $PbTiO_3$ thin films can be switched via changes in pO_2 [5]. More generally, the dependence of the piezoelectric character of epitaxial ferroelectric films, in particular $PbZr_{1-x}Ti_xO_3$ thin films has been the subject of many works dating back to the 1990s [6,7].

However, less work has been reported on the thickness-dependent properties of epitaxial BTO thin films [8]. Comparably, much more literature exists in BTO ceramics and dependence of electrical and dielectric properties on their grain size, or the dependence on the strain state [9–11]. One of the challenges with BTO is that thin films often suffer from high leakage current, making measurements more difficult. In a further complication, piezoresponse force microscopy (PFM) which is the primary tool of choice for measurements of the converse piezoelectric coefficients, is known to be heavily influenced by spurious contributions that make calibration and reliable, quantitative measurements a difficult undertaking [12,13]. The second challenge lies in interpretation of the thickness dependence results. Because many variables (such as strain, composition, defects) that can influence the ferroelectric properties are also thickness-dependent, understanding the underlying mechanisms that drive the thickness-dependence observed requires structural characterization and local quantitative measurements, in addition to modeling.

Here, we address this gap in the literature via a study of the converse piezoelectric coefficients of heteroepitaxial BTO thin films. Films were grown via pulsed laser deposition on 5 nm $SrRuO_3$//$SrTiO_3$ single crystal substrate of a thickness series ranging from 10 to 80 nm. We perform structural characterization including atomic force microscopy (AFM), and reciprocal space mapping with x-ray diffraction, to understand the thickness-structure dependence of the series. By varying the film thickness, we successfully strain engineer the BTO due to lattice mismatch of the underlying substrate. We then perform quantitative measurements of the d_{33} via interferometric displacement sensing (IDS) in a coupled AFM system. IDS allows for the extraction of a vibration amplitude at a given frequency based on a doppler shift of the laser reflected off the AFM cantilever. In principle, IDS enables accurate tip displacement measurements while virtually eliminating any spurious electrostatic contributions [14]. Additionally, we acquire hysteresis loops via band excitation piezoresponse force microscopy (PFM) to probe the hysteretic-thickness behavior [15]. Reactive-force field (ReaxFF)-based molecular

*These authors contributed equally to this work.
†ganeshp@ornl.gov

Published by the American Physical Society under the terms of the Creative Commons Attribution 4.0 International license. Further distribution of this work must maintain attribution to the author(s) and the published article's title, journal citation, and DOI.

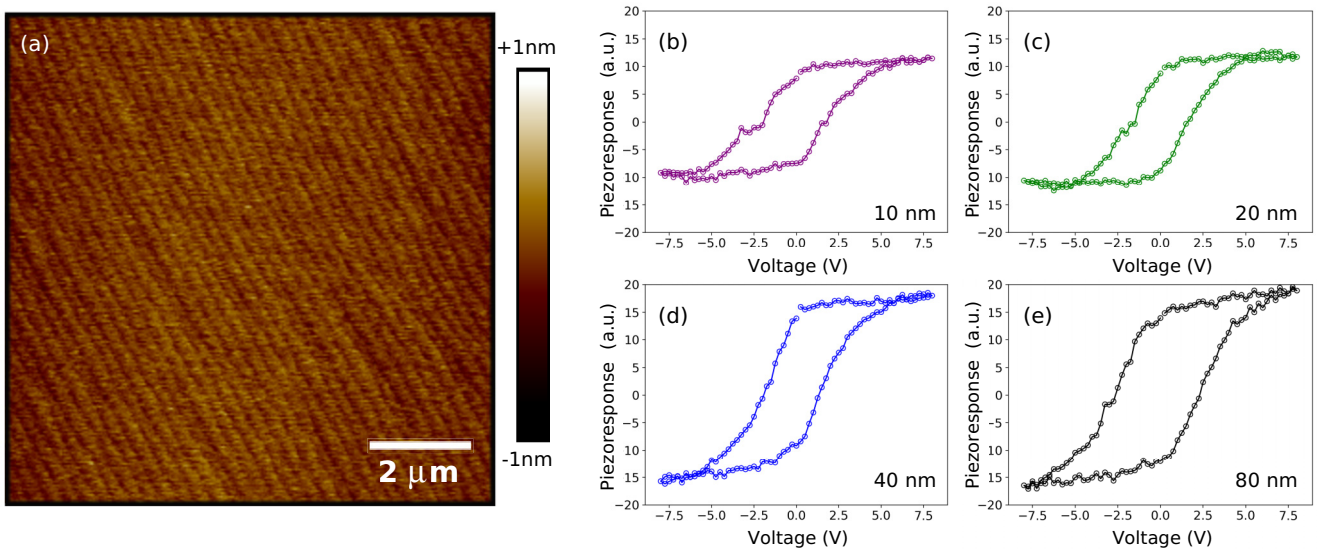

FIG. 1. (a) Representative atomic force microscopy of $BaTiO_3$ thin film grown on 5 nm $SrRuO_3$//$SrTiO_3$ single crystal substrate. (b)–(e) Band excitation piezo force spectroscopy of $BaTiO_3$ thin films with varying thickness, 10–80 nm. PFM loops are averages on three triangle waves with an amplitude of 8 V.

dynamics (MD) simulations were carried out to provide an accurate atomistic level description of chemistry and dynamics of the system. ReaxFF was initially designed for hydrocarbon systems and later successfully applied to several other materials such as metals, ceramics, polymer systems and two-dimensional materials [16–23]. In this work, we use the recently developed fully *ab initio* derived atomistic ReaxFF for BTO thin films, which naturally captures local inhomogeneous strain and polarization gradients, implicitly containing higher-order couplings important for field responses and understanding ferroelectric properties [24].

II. RESULTS AND DISSCUSSION

The representative surface morphology of BTO thin films measured via AFM is shown in Fig. 1(a). Typical step and terrace morphology is observed with a surface roughness of less than 1 nm corresponding to unit cell surface structures, providing an ideal platform for surface probe microscopy measurements. PFM band excitation voltage spectroscopy results, with voltages ranging from −8V to +8V, are shown in Figs. 1(b)–1(e) displaying BTO's piezoresponse as a function of thickness (and thus strain). Note, the corresponding amplitude and phase signals can be found in the Supplemental Material [25] (Fig. S1). Increasing the thickness from 10 to 80 nm reveals a twofold increase in piezoresponse, accompanied by a decrease in compressive in-plane strain (Fig. 2). As evident from PFM, all thicknesses exhibit clear hysteretic behavior. However, since the PFM signal contains multiple contributions including from electrostatics and piezoelectric modulus (which complicates interpretation) [12], we have employed IDS to quantitatively measure the piezoresponse of the sample and eliminate unwanted signals arising from electrostatic effects and cantilever motion [26].

Figure 2(a) shows the converse piezoelectric coefficient d_{33} as measured via IDS and the corresponding lattice strain [Fig. 2(b)] as determined from XRD with varying thin film thickness. The converse piezoelectric coefficient shows a strong dependence on the film thickness in the $1-3\,V_{ac}$ range, with a maximum of $20.5\,pm\,V^{-1}$ at 80 nm. Below 20 nm, the d_{33} approaches the detection limit of IDS which is approximately $\sim$1 pm. The in-plane epitaxial strain shows an inverse dependence on thin film thickness increasing from fully relaxed to −2.05%.[1]

It is noteworthy that from 20 to 40 nm, the strain remains relatively constant while the converse piezoelectric coefficient increases to 9.6 pm/V, which suggests the onset of dominating interface effects or frozen dead layer consistent with previous reports exploring scaling effects in ferroelectrics [8,27,28]. The connection between d_{33} values and in-plane strain strongly suggest that in addition to the interfacial layer, increased compressive strain drives reduction in the observed piezoelectric properties.

For completeness, it is important to point out the effects of non-uniform electric fields present during PFM based techniques; thus, we also plot the following analytical equation for a point-charge-like model for non-uniform electric fields in tetragonal piezoelectric films (Fig. 2(a), blue), referred to as the effective converse piezoelectric coefficient d_{33}^{eff} [29]:

$$d_{33}^{\text{eff}} \approx -\frac{\gamma^2 h^2}{[h+\gamma(d+h)]^2} d_{15} - \frac{h[h+(d+2h)\gamma]}{[h+\gamma(d+h]^2} d_{33} - \left(\frac{(1+2\nu)h}{h+\gamma(d+h)} - \frac{\gamma h^2}{[h+\gamma(d+h)]^2}\right) d_{31}, \quad (1)$$

[1]Note, the XRD reciprocal space map for the 80 nm film (Fig. S2d [25]) shows an additional strain component corresponding to a highly strained interface layer (similar to 10 nm). For in-plane strain calculations, this strain layer was ignored as it is assumed majority of the film is in a relaxed state.

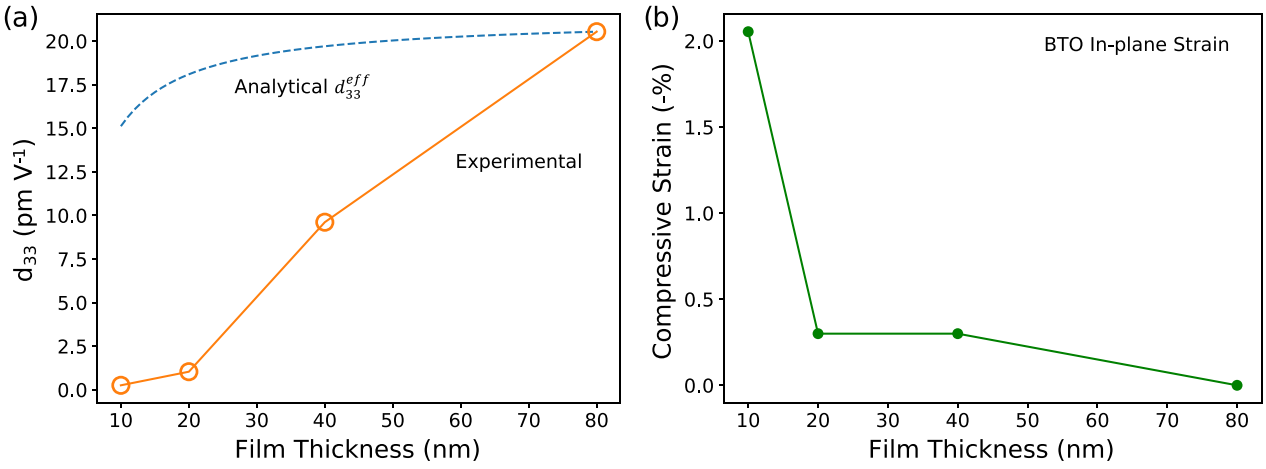

FIG. 2. (a) Effective converse piezoelectric coefficient $d_{33}{}^{\text{eff}}$ versus film thickness for experimental (orange) and analytical solution (blue). Note, analytical equation has been shifted to overlay experimental 80-nm point (original in Fig. S6 [25]). (b) Compressive in-plane lattice strain as a function of $BaTiO_3$ thickness.

where $\gamma = \sqrt{\varepsilon_{33}/\varepsilon_{11}}$ is the dielectric anisotropy factor of the film, h is the film thickness, ν is Poission's ratio (typically 0.25–0.35), d_{ij} is the converse piezoelectric tensor, $d = 2R_o/\pi$ is the effective point charge distance from the surface, and R is the probe-surface contact radius (see Supplemental Material for calculation details [25]). As seen from Fig. 2(a) (blue dashed), the change in d_{33}^{eff} over the range of thicknesses is on the order 5 pm/V indicating the observed decrease in experimental d_{33} values is attributed to more than extrinsic size effects.[2]

To complement strain-dependent converse piezoelectric coefficients extracted from IDS, Figs. 3 and 4 show ReaxFF simulations of BTO under different strain states. Experimentally, the film thickness and strain state are coupled with an inverse dependence (Fig. 2), and it appears that it is the increase in compressive strain that causes the reduction in d_{33}. To capture this in our simulations, the lattice parameter was varied uniformly to produce a specific strain state comparable to experiments, to a [001] oriented BTO thin-film with a constant thickness of 32 nm. In our setup, the z direction is normal to the thin film surfaces with Ba-O terminated and Ti-O terminated [001] surfaces on the positive and negative z side of the film, respectively. The cation asymmetry at the interfaces allows for the formation of a dipole moment, and consequently a ferroelectric 180° domain wall, due to the two interfaces having opposite dipole moments. This 180° domain wall ground-state structure is what we expect in a thin-film with two free uncompensating surfaces, as it minimizes the net "depolarizing field," i.e., the field opposite to bulk polarization produced by uncompensated surface polarization charges in a uniformly poled film.

Figure 3 shows the domain evolution with an applied electric field for three different strain states: -2%, -1%, and 0% compressively strained (finer electric field increments shown in Fig. S5 [25]). With no applied electric field, the thickness of the domain wall was calculated to be approximately 2.5 nm with saturated dipole moments (or equivalently the polarization) of 18.6 μC/cm^2 [Fig. 3(a), left] and 20.2 μC/cm^2 [Fig. 3(c), left] for relaxed and -2% strained states, respectively. Increase in the saturation polarization value with compressive strain is consistent with earlier full *ab initio* studies on thinner films [30]. Applying an electric field of 0.1 V/nm along $+z$ direction resulted in the domain wall moving to the top surface with the rest of the film aligning the dipoles along the field direction. With an applied electric field of 0.1 V/nm, for the relaxed case [Fig. 3(a), right], the dipole-moment corresponding to the polarization at the top-surface $P_{z,\text{surface}}$ was pinned pointing opposite to the field-direction, at a value of -8.8 μC/cm^2; however, for the -2% strained film [Fig. 3(c), right], the moment at the top-surface was pinned at -13.5 μC/cm^2 (a 54% increase in polarization compared to that in the relaxed state). The presence of a surface polarization layer pointing "opposite" to the field direction as observed in our simulations is due to an increase in the depolarizing-field in the uniformly poled sample, resulting in a ferroelectric "dead-layer," which is difficult to switch, consistent with earlier first-principles based simulations on thinner films [31]. Since our method allows us to model thicker films than those possible using full *ab initio* methods, we can further estimate how the thickness of the layer screening the depolarizing field (i.e., the screening-layer) evolves with strain. As seen in Fig. 3, in the case of the -2% strained film, the polarization gradient extends 2.3 nm further into the film, compared to the unstrained case. A larger screening-layer should result in more energy to switch the polarization with external fields, leading to a smaller piezoelectric response. To quantify the effect of this increased screening-layer on the piezoelectric response of the film, we calculate the converse piezoelectric coefficient d_{33} component for different strained films and compare the trend with the experimental trend as shown in Fig. 2.

We calculated d_{33}, by computing the slope of the average displacement of the thin film along the [001] direction as a function of applied voltage, in the range of 0–10 V, as shown

[2]The analytical calculation plotted in Fig. 2(a) has been shifted down to overlay the experimental 80-nm point (original in Fig. S6 [25]).

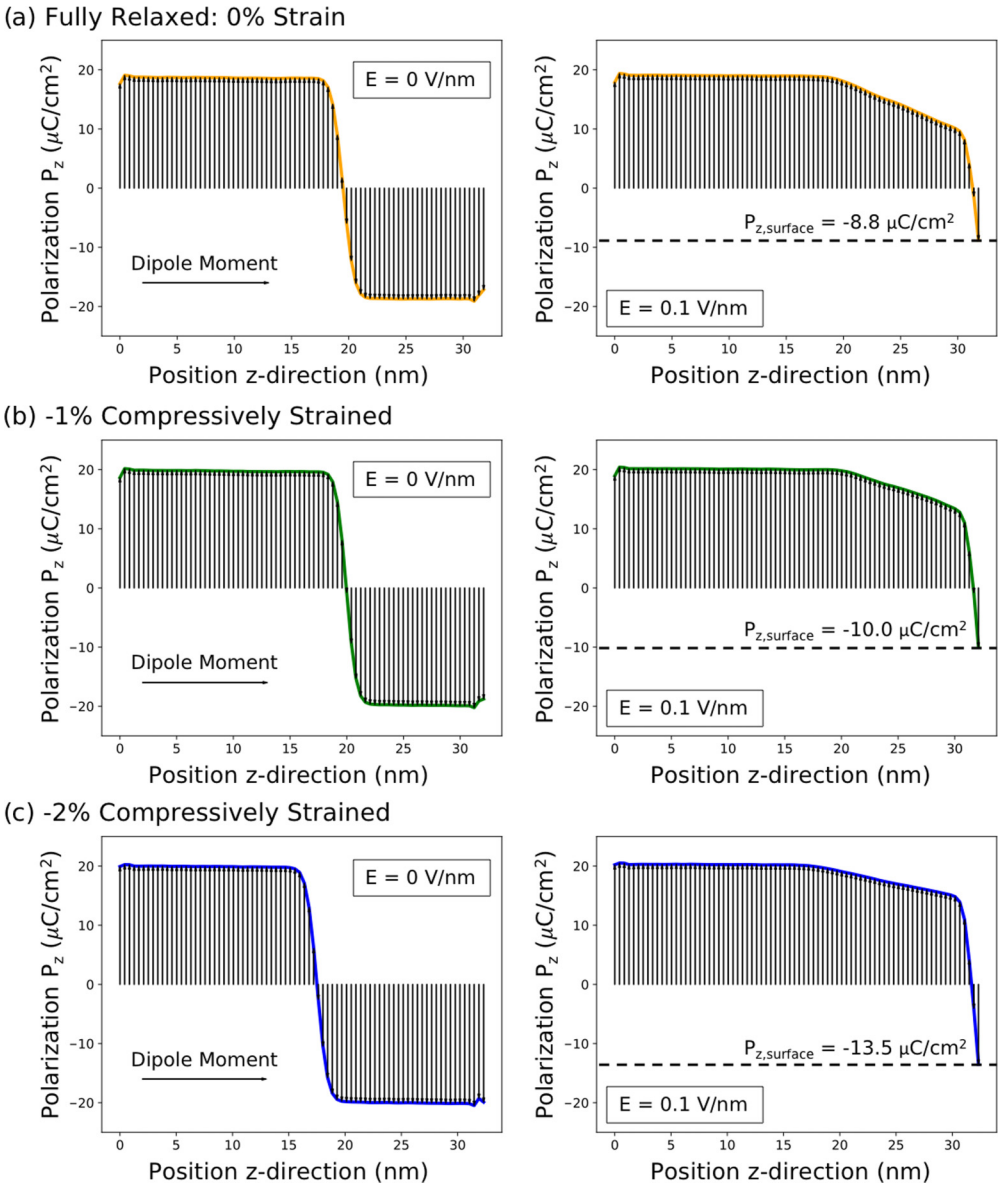

FIG. 3. ReaxFF molecular dynamics simulations of local polarization along [001]-direction of (a) relaxed film, (b) -1% compressively strained film, and (c) -2% compressively strained film with applied electric field ranging 0.0 V/nm to 0.1 V/nm. Vertical arrows indicate direction of the dipole moment inside the film and $P_{z,\text{surface}}$ denotes surface polarization. Note, simulated thickness is 32 nm (80 unit cells).

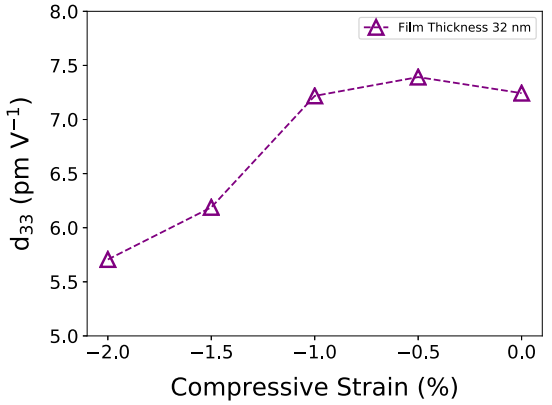

FIG. 4. Converse piezoelectric coefficient d_{33} of 32 nm $BaTiO_3$ thin films calculated using ReaxFF molecular dynamic simulations.

in Fig. S4 [25]. As Fig. 4 shows, d_{33} decreases with increasing compressive strain, in good agreement with our experimental observations shown earlier in Fig. 2. ReaxFF simulations therefore accurately capture the experimentally observed trend via IDS measurements and also successfully predict a plausible mechanism for it, in terms of an increasing thickness of the screening-layer. It should be noted that in the real material, there could be other compensating mechanism for the depolarizing fields, that are not included in the model—such as electronic effects, or defects—both intrinsic as well as extrinsic. While electronic reconstructions cannot be explicitly considered in the ReaxFF methodology; our force field is developed to describe complex defect chemistries. Studies exploring how intrinsic as well as extrinsic (mobile and charged) defects influence this trend are ongoing. The precise interplay of which screening mechanism (structural,

electronic, ionic, etc.) are observed will depend on relative energetics of each process. It would therefore be instructive for controlled screening by chemical dosing to better explore the ferroionic phase diagram [3].

III. CONCLUSION

In this study, we grew epitaxial BTO of decreasing thickness via pulsed laser deposition and quantitatively measured the d_{33} and strain states. We observed strong correlation between strain and converse piezoelectric coefficient. Structural and surface characterization reveal a thickness dependent in-plane strain and consistent step-terrace surface morphology. The effects of strain due to lattice mismatch can be seen in IDS measurements with a d_{33} of 20.5 pmV^{-1} at 80 nm, which continuously declines with increasing in-plane strain. Based on ReaxFF simulations, we posit the piezoelectric tensor's dependence on strain is related to a frozen interface layer and increasing screening-layer with compressive strain. Our results show IDS in conjunction with ReaxFF modeling is a useful tool in understanding scaling effects in ferroelectric thin films.

IV. EXPERIMENTAL METHODS

A. Growth and characterization

All films were grown via pulsed laser deposition at 700 °C in 99.9999% pure O_2 using (100) single sided epitaxial-polished $SrTiO_3$ substrates. First, a $SrRuO_3$ layer (<5 nm), which serves as the bottom electrode for electrical measurements, was grown at 100 millitorr with a laser pulse rate of 5 Hz from a stoichiometric SrRuO3 ceramic target. Subsequently, $BaTiO_3$ of various thicknesses were grown at 10 millitorr with a laser pulse rate of 10 Hz from a stoichiometric $BaTiO_3$ target. The fluence for both thin film layers was maintained at approximately 1.2 $\mathrm{J/cm}^2$. Substrates were prepared by sonication in a warm (∼70 °C) deionized water bath for 1 min followed by an anneal at 1000 °C for 12 h to produce TiO_2 termination, and step/terrace surface morphology.

Interferometric displacement sensor measurements were taken using an Oxford Instruments Cypher atomic force microscope equipped with a Polytec OFV-5000 Modular Vibrometer routed to the tip for measuring tip displacements, i.e., converse piezoelectric coefficient d_{33}. AC voltages ranging from 0.5 to 3 V at 400 kHz were used for d_{33} calculations. An average displacement from 256 points at each AC voltage was used in calculating the d_{33} value. Furthermore, the Cypher AFM using optical beam deflection in tapping mode was implemented for surface characterization. Piezo force microscopy (PFM) measurements were taken using band excitation frequency tracking to acquire the true contact resonance and mitigate crosstalk. Details describing band excitation functionality can be found elsewhere [15]. Stepped on-off triangle voltage waves were applied to the AFM cantilever with an amplitude of 8 V and frequency of 0.25 Hz. Further, Figs. 1(b)–1(e) PFM loops were taken from an average of three cycles. Note, the same AFM cantilever (Budget Sensors Electri Muli75-G Cr/Pt) was used in measuring all PFM loops to minimize variations between measurements.

Crystal quality was characterized by reciprocal space mapping (Fig. S2 [25]) in an asymmetric geometry using a Panalytical X'pert diffractometer with a double bounce monochromated beam optic and parallel plate collimator (0.18°). The lattice parameters were calculated using a pseudo-cubic approximation of the $BaTiO_3$ 103 diffraction peak. Additionally, thicknesses were measured by x-ray reflectivity (XRR) with the aforementioned optics.

B. ReaxFF molecular dynamics modeling

Large-scale Atomic/Molecular Massively Parallel Simulator (LAMMPS) [32] with ReaxFF implementation [33] was utilized for reactive molecular dynamics (MD) simulations. Supercells were built as 4×4 nm in x and y directions. Thickness of the film varied from 16 to 32 nm with supercell contains 20 000 to 40 000 atoms, respectively. Temperature kept constant using Berendsen thermostat [34]. Periodic boundary conditions applied in x and y directions and a 2 nm vacuum space was considered on the top and bottom regions of the film. The strain applied via deforming the super cell in x and y directions. MD timestep was set to 0.25 fs.

First, temperature ramped up from 0 to 300 K in 7.5 ps and kept at 300 K for 5.0 ps. Second, system was cooled down to 0 K in 7.5 ps and then heated up back to 150 K for another 5.0 ps to recover dipole moments. At 150 K, electric field in z direction was applied on the system. The magnitude of the field increased from 0.0 to 0.03 V/A with 0.01 V/A increments in 7.5 ps for each step. Data was collected in the last 0.5 ps of each step.

At the data collection stage, z coordinates of Ba atoms were recorded and time averaged. Ti centered unit cell for $BaTiO_3$ were chosen with Ba atoms located at the corners. Average z coordinates of Ba atoms were binned to generate histogram plot. Thickness of individual monolayers was calculated based on the distance between peaks in histogram plot.

Classical charges on each atom were calculated using electron equilibration method (EEM) in ReaxFF at every step of the simulation. Charges and positions were recorded every 500 steps during the simulation to calculate the unit cell polarization defined as

$$P_u(t) = \frac{1}{V_u}\left(Z^*_{\mathrm{Ti}} r_{\mathrm{Ti}}(t) + \frac{1}{8} Z^*_{\mathrm{Ba}} \sum_{i=1}^{8} r_{\mathrm{Ba},i}(t) + \frac{1}{2} Z^*_{O} \sum_{i=1}^{6} r_{O,i}(t)\right).$$

Here, Z_{Ti}, Z_{Ba}, and Z_O are classical charges and V_U is the unit-cell volume. Since Ba atoms located at corners in the unitcell, the volume was calculated using positions of Ba atoms with Convex Hull algorithm provided with SciPy package.

ACKNOWLEDGMENTS

The work was supported by the U.S. Department of Energy, Office of Science, Materials Sciences and Engineering Division (K.P.K., R.K.V., Y.S., and H.N.L.). The PFM and portion of the modeling work was conducted at and supported (PG) by the Center for Nanophase Materials Sciences, which is a DOE Office of Science User Facility. Computations used resources of the National Energy Research Scientific Computing Center (NERSC), a U.S. Department of Energy

Office of Science User Facility operated under Contract No. DE-AC02-05CH11231. D.Y., D.A., and A.C.T.v.D. would like to acknowledge Grant No. AFRL FA9451-16-1-0041 and AFOSR MURI Contract No. FA9550-19-1-0008.

This manuscript has been authored by UT-Battelle, LLC, under Contract No. DE-AC0500OR22725 with the U.S. Department of Energy. The United States Government retains and the publisher, by accepting the article for publication, acknowledges that the United States Government retains a nonexclusive, paid-up, irrevocable, world-wide license to publish or reproduce the published form of this manuscript, or allow others to do so, for the United States Government purposes. The Department of Energy will provide public access to these results of federally sponsored research in accordance with the DOE Public Access Plan (http://energy.gov/downloads/doe-public-access-plan).

[1] D. G. Schlom, L. Chen, C. Eom, K. Rabe, S. K. Streiffer, and J. Triscone, Rev. Mater. Res. **37**, 589 (2007).
[2] N. Setter and D. Damjanovic, J. Appl. Phys. **100**, 051606 (2006).
[3] A. N. Morozovska, E. A. Eliseev, N. V. Morozovsky, and S. V. Kalinin, Phys. Rev. B **95**, 195413 (2017).
[4] S. M. Yang, A. N. Morozovska, R. Kumar, E. A. Eliseev, Y. Cao, L. Mazet, N. Balke, S. Jesse, R. K. Vasudevan, C. Dubourdieu, and S. V. Kalinin, Nat. Phys. **13**, 812 (2017).
[5] R. V. Wang, D. D. Fong, F. Jiang, M. J. Highland, P. H. Fuoss, C. Thompson, A. M. Kolpak, J. A. Eastman, S. K. Streiffer, A. M. Rappe, and G. B. Stephenson, Phys. Rev. Lett. **102**, 047601 (2009).
[6] D. M. Kim and C. B. Eom, Appl. Phys. Lett. **88**, 142904, (2006).
[7] K. Udayakumar, P. Schuele, J. Chen, S. Krupanidhi, and L. Cross, J. Appl. Phys. **77**, 3981 (1995).
[8] Y. Guo, K. Suzuki, K. Nishizawa, T. Miki, and K. Kato, Japan. J. Appl. Phys. **45**, 855 (2006).
[9] C. Ederer and N. A. Spaldin, Phys. Rev. Lett. **95**, 257601 (2005).
[10] A. R. Damodaran, E. Breckenfeld, Z. Chen, S. Lee, and L. W. Martin, Adv. Mater. **26**, 6341 (2014).
[11] K. J. Choi, M. Biegalski, Y. L. Li, A. Sharan, J. Schubert, R. Uecker, P. Reiche, Y. B. Chen, X. Q. Pan, V. Gopalan, L. Chen, D. G. Schlom, and C. B. Eom, Science **306**, 1005 (2004).
[12] R. K. Vasudevan, N. Balke, P. Maksymovych, S. Jesse, and S. V. Kalinin, Appl. Phys. Rev. **4**, 021302 (2017).
[13] N. Balke, S. Jesse, P. Yu, B. Carmichael, S. V. Kalinin, and A. Tselev, Nanotechnology **27**, 425707 (2016).
[14] A. Labuda and R. Proksch, Appl. Phys. Lett. **106**, 253103 (2015).
[15] S. Jesse, S. V. Kalinin, R. Proksch, A. P. Baddorf, and B. J. Rodriguez, Nanotechnology **18**, 435503 (2007).
[16] A. C. T. van Duin, S. Dasgupta, F. Lorant, and W. Goddard, J. Phys. Chem. A **105**, 9396 (2001).
[17] D. E. Yilmaz, Comput. Mater. Sci. **109**, 183 (2015).
[18] D. E. Yilmaz and A. C. T. van Duin, Polymer **154**, 172, (2018).
[19] D. E. Yilmaz, R. Lotfi, C. Ashraf, S. Hong, and A. C. T. van Duin, J. Phys. Chem. C **122**, 11911 (2018).
[20] R. Lotfi, M. Naguib, D. E. Yilmaz, J. Nanda, and A. C. T. van Duin, J. Mater. Chem. A **6**, 12733 (2018).
[21] N. C. Osti, M. Naguib, A. Ostadossein, Y. Xie, P. R. C. Kent, B. Dyatkin, G. Rother, W. T. Heller, and A. C. T. van Duin, ACS Appl. Mater. Interfaces **8**, 8859 (2016).
[22] D. Akbarian, D. E. Yilmaz, Y. Cao, P. Ganesh, I. Dabo, J. Munro, R. V. Ginhoven, and A. C. T. van Duin, Phys. Chem. Chem. Phys. **21**, 18240, (2019).
[23] M. Kowalik, C. Ashraf, B. Damirchi, D. Akbarian, S. Rajabpour, and A. C. T. van Duin, J. Phys. Chem. B **123**, 5357 (2019).
[24] D. Akbarian, H. Hamedi, B. Damirchi, D. E. Yilmaz, K. Penrod, W. H. Woodward, M. Lanagan, and A. C. T. van Duin, Polymer **183**, 121901 (2019).
[25] See Supplemental Material at http://link.aps.org/supplemental/10.1103/PhysRevMaterials.4.024407 for additional experimental details and materials characterization.
[26] L. Collins, Y. Liu, O. S. Ovchinnikova, and R. Proksch, ACS Nano **13**, 8055 (2019).
[27] P. Padmini, T. R. Taylor, M. J. Lefevre, A. S. Nagra, R. A. York, and J. S. Speck, Appl. Phys. Lett. **75**, 3186 (1999).
[28] O. Vendik and S. Zubko, J. Appl. Phys. **88**, 5343 (2000).
[29] A. N. Morozovska, S. v. Svechnikov, E. A. Eliseev, and S. V. Kalinin, Phys. Rev. B **76**, 054123 (2007).
[30] A. Tariq and S. Nazir, AIP Adv. **7**, 115211 (2017).
[31] Y. Wang, M. K. Niranjan, K. Janicka, J. P. Velev, M. Y. Zhuravlev, S. S. Jaswal, and E. Y. Tsymbal, Phys. Rev. B **82**, 094114 (2010).
[32] S. Plimpton, J. Comput. Phys. **117**, 1,(1995).
[33] H. M. Aktulga, J. C. Fogarty, S. A Pandit, and A. Y. Grama, Parallel Comput. **38**, 245 (2012).
[34] H. J. C. Berendsen, J. P. M. Postma, W. F. Van Gunsteren, A. DiNola, and J. R. Haak, J. Chem. Phys. **81**, 3684 (1984).